

Mapping out electron–electron interactions in angular space

F O Schumann¹, C Winkler and J Kirschner

Max-Planck Institute of Microstructure Physics, Weinberg 2,
06120 Halle, Germany
E-mail: schumann@mpi-halle.de

New Journal of Physics **9** (2007) 372

Received 27 June 2007

Published 12 October 2007

Online at <http://www.njp.org/>

doi:10.1088/1367-2630/9/10/372

Abstract. Many-body effects in solids are related to the correlation among electrons. This mutual interaction between the electrons can be probed by electron pair emission spectroscopy. We have investigated the electron pair emission from a LiF(100) surface upon excitation with low kinetic energy electrons. Our angular distributions clearly show that the emission direction of one electron is surrounded by a reduced intensity of the other electron. This depletion zone of electronic intensity is a manifestation of the exchange and correlation hole. We show that we are able to observe the full extension and shape of the depletion zone. It has an angular extension of ≈ 1.2 rad and is independent of the electron energy. Additionally, we discovered that the angle between the trajectories of the electrons has a profound effect on the two-dimensional energy distribution.

Contents

1. Introduction	2
2. Experiment	3
3. Normal incidence excitation	6
4. Non-normal incidence excitation	8
5. Discussion	13
6. Summary	13
Acknowledgments	14
References	14

¹ Author to whom any correspondence should be addressed.

1. Introduction

Electronic transport is an integral part of modern technology, if we recall microelectronics for example. First attempts to describe the phenomenon of electrical conductivity in metals can be traced back to the work of Drude [1] and Lorentz [2]. The physical picture they devised was based on the assumption that the electrons do not interact in the metal and that only elastic collisions occur at the positions of the atoms. In an applied electrical field, these collisions ensure that the velocity of the electrons converges to a constant value. This rather crude theory gave a satisfactory explanation of the finite resistivity and the observed Ohm's law. However, the application of the classical kinetic gas theory failed completely to describe the behavior of the specific heat. The linear temperature dependence of the electronic specific heat at low temperatures could be accounted for in the so-called Sommerfeld theory [3]. Again electrons were treated as independent and non-interacting particles, but the rules of quantum mechanics were used, most important was the inclusion of the Fermi–Dirac statistics. Electrons in a solid, however, do not move independently of each other, they experience a mutual force mediated by the Coulomb interaction. Hence one would expect the independent electron picture to be an inadequate description of electrons in a solid. This apparent contradiction could be resolved by the fundamental work of Wigner and Seitz [4] and Slater [5], introduced more than 70 years ago. This can be understood by recalling that the Pauli principle demands that two electrons cannot be at the same location if they have parallel spins. The Coulomb interaction makes it energetically more favorable for electrons to be separated. The net effect is that each electron is surrounded by a missing electronic charge, this electronic depletion zone has been termed as the exchange-correlation (xc)-hole. The xc-hole has a spatial extension of the order of a few ångström and amounts to exactly the charge of an electron. This means that over distances larger than the size of the xc-hole each electron is screened from the other electrons. Another description would be to regard the electron and the xc-hole as a ‘quasi-particle’ with no charge. The work of Wigner and Seitz and Slater explains why the approximation of Lorenz, Drude and Sommerfeld, namely a non-interacting electron gas, can give reasonable results. However, it is clear that many-body phenomena like magnetism, superconductivity and heavy fermions to name a few are beyond the independent electron picture. The determination of the ground state wavefunction of interacting electrons in a macroscopic sample is a hopeless task. A major breakthrough in the description of the ground state properties of condensed matter was therefore the development of the density functional theory (DFT) [6]–[8]. It was shown that the ground state energy is a functional of the electron density $n(\mathbf{r})$, likewise all other ground state properties are exactly described by the functionals of $n(\mathbf{r})$. This concept can be put into a computational scheme by the local density approximation (LDA) leading to the Kohn–Sham equation, which formally looks like a Schrödinger equation of a single particle moving in an effective potential [6]–[8]. An important contribution to this potential comes from $\delta E_{xc}/\delta n(\mathbf{r})$, where the functional E_{xc} contains all features of the interacting electronic system. Key quantities for E_{xc} are the pair correlation function $\mathbf{g}(\mathbf{r}, \mathbf{r}')$ and the xc-hole (function) $\mathbf{n}_{xc}(\mathbf{r}, \mathbf{r}')$. The first quantity is the probability to find an electron at coordinates \mathbf{r} , when a second is located at \mathbf{r}' [4, 5, 9]. As discussed before, \mathbf{g} is essentially constant (normalized to 1) except for small distances $|\mathbf{r} - \mathbf{r}'|$ of the order of a few ångström, where \mathbf{g} adopts smaller values. The term xc-hole is linked to the pair correlation function via $\mathbf{n}_{xc}(\mathbf{r}, \mathbf{r}') = \mathbf{n}(\mathbf{r}')[\mathbf{g}(\mathbf{r}, \mathbf{r}') - 1]$. Simply put, the LDA, a very successful description for condensed matter, incorporates the xc hole. Different approaches have been put forward to improve the LDA calculations via

different choices for $\mathbf{n}_{xc}(\mathbf{r}, \mathbf{r}')$ [10]–[15]. It would be therefore desirable to access the key function $\mathbf{n}_{xc}(\mathbf{r}, \mathbf{r}')$ via experiment. This is not yet directly possible, but we are able to measure the angular distribution. Due to the electron–electron interaction, electrons will scatter from each other while moving in the solid. Scattering is also the key to studying the electron–electron interaction, and scattering experiments have a long tradition in physics. The angular distributions of the projectile have been used to study the interaction between projectile and target. We recall the landmark experiments by Rutherford and co-workers, their angular distribution of the scattered α particles led to the discovery that most of the mass of an atom is confined in a small region of space. Clearly, studying the electron–electron interaction via a scattering experiment is most appropriate [16]. Our experimental approach reflects this argument and we excite the solid surface via a primary electron beam and measure the angular distribution of the emitted electron pairs. Recent advances on the experimental side have made it possible to address the aforementioned concept of the xc-hole [17, 18]. In this paper, we show that it is experimentally possible to measure the full angular distribution of the electron pairs ejected from a solid surface. Our studies highlight the fact that the xc-hole is an experimental reality.

2. Experiment

Before we discuss our experiment in detail, a few general statements about our experimental approach are in order. Our goal is to study the electron–electron interaction in solids and the size of the exclusion zone or xc-hole. The most obvious experiment is to perform a scattering experiment in the spirit of Rutherford. Applied to our situation, we need to study the collision between two electrons after a primary electron hits the sample. We may term such an experiment as an (e, 2e) process. The detection of electron pairs is a straightforward, although experimentally demanding, extension of single electron spectroscopy. The following approaches are conceivable, a transmission experiment would require a large kinetic energy of the primary electron, of the order of 20–100 kV, to pass through a thin foil. Such experiments have been indeed performed and have given useful insights into the spectral momentum density [19, 20]. The equivalent experiment in a reflection geometry is also possible, where the primary electron has an kinetic energy of 300 eV [21]. Both approaches choose the kinematics such that the scattered primary electron loses a small fraction of its kinetic energy, hence the second electron has a much smaller kinetic energy than the scattered primary. Further the momentum transfer of the primary electron is very small. This constitutes the so-called optical-limit, where the primary electron acts like a photon [22]. This allowed comparison with photoemission results. Over the past decade it has been demonstrated that experiments in a reflection geometry employing primaries with energies of 30 eV are possible, which were not confined to the optical limit [23]–[25]. In parallel to the experimental advances the theoretical description of the (e, 2e) process made significant progress, too [24], [26]–[29]. The low kinetic energy reflection geometry adapts better to our aims than the high kinetic energy transmission geometry. The energy introduced to the system by the primary electron needs to be compared with the energies relevant for electron–electron correlation. Within the Hubbard model, the strength of the electron correlation is described by the parameter U , which is of the order of a few electron volts. Clearly, the energetics of a transmission experiment is too high to be sensitive to the electron–electron interaction in contrast to a low kinetic energy experiment. The key for a successful reflection experiment is a high probability of reflection, which is

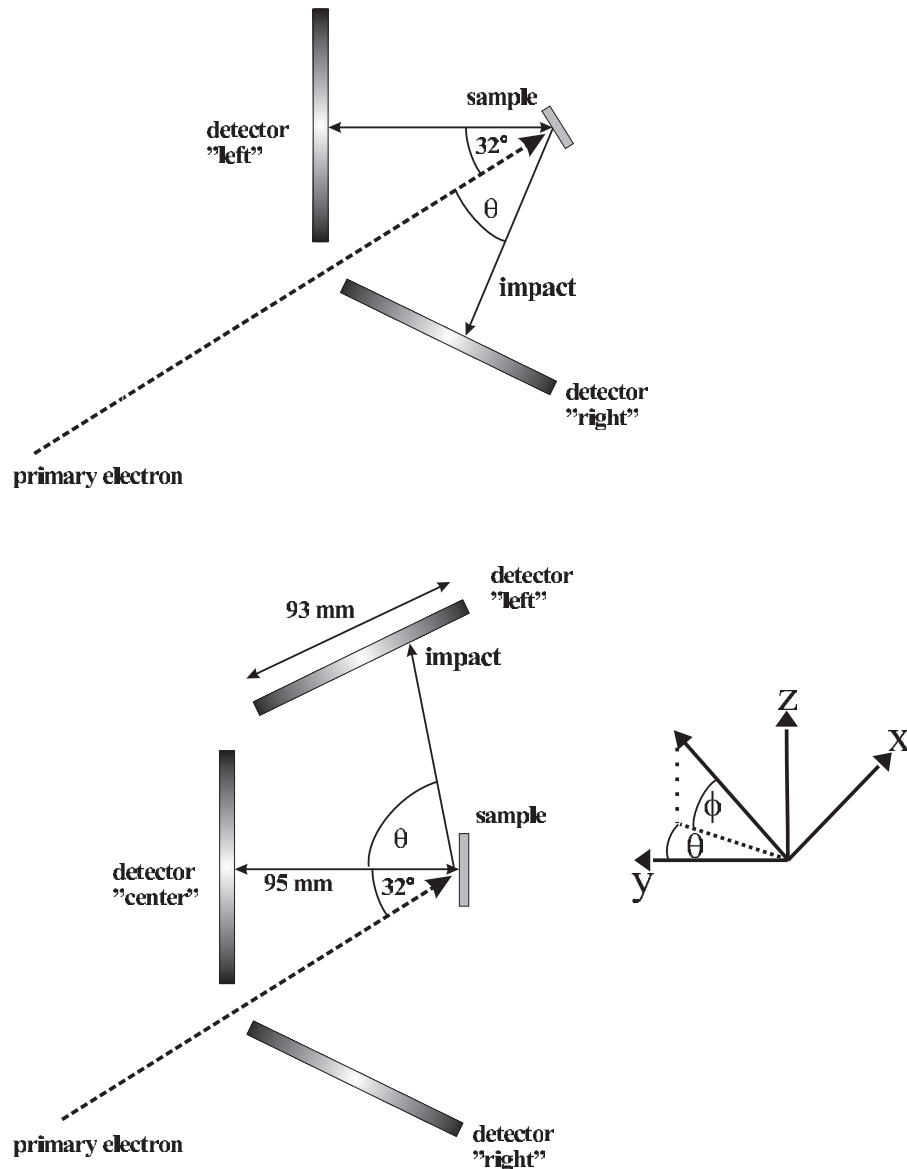


Figure 1. Sketch of the employed geometries and definition of the angles Θ and Φ .

demonstrated by the widely used technique of low electron energy diffraction (LEED). The primary electron is reflected back elastically, though energy losses via excitations of plasmons, phonons, exciton etc are possible and have been observed in electron energy loss spectroscopy (EELS). However, the contribution of the losses compared to the elastic peak is orders of magnitude smaller. The key result is that one can regard the reflection experiment we perform as a kind of transmission experiment through the topmost layers, where the reflected primary beam has a well-defined energy and momentum. Clearly, such an experiment will have a small cross-section: electrons in a solid try to avoid scattering from each other, up to ‘disguising’ themselves as neutral quasi-particles. This means that our experiments observe only that small fraction of scattering events where two quasi particles come sufficiently close (i.e. less than

the screening length) to ‘feel’ each other. In figure 1, we provide a schematic view of our time-of-flight (TOF) experimental set-up and the two geometries employed. The electron gun uses a BaO cathode and with that the overall energy spread is 0.4 eV. The pulsing is achieved via electro-static deflection of the electron beam across a small aperture within the gun. Pulse widths of 0.5 ns can be achieved at a repetition rate of 2 MHz. The primary current on to the sample is about 10^{-14} A. By performing LEED with our set-up the width of the diffraction spots are defined by the angular divergence of the gun. This is usually expressed in terms of the transfer width, we calculate a value of 140 \AA^{-1} . A coincidence circuit ensures that only electron pairs emitted from the surface are being registered thereby suppressing the large contribution of single electron emission. The TOF of the electrons depends on the energy and the emission direction, since the latter defines the actual length of the flight path. When the two electrons forming the pair leave the sample, they will have in general different energies and different flight paths. Consequently the electrons will reach the detectors at different times. For example, an electron of 30.7 eV (elastically scattered primary) has a TOF of about 30 ns, an electron with 2 eV (our low kinetic energy cut-off) travels for about 110 ns. This means that the TOF difference of electrons forming a pair has to be lower than 80 ns. The first electron to hit the detector will define electronically a time window in which the second electron has to hit the detector. Only in this case, we consider it to be a valid coincidence event. This concept only works if we ensure that only one pair exists after the excitation. This can be realized experimentally by operating with a low primary beam. We use for normal incidence of the primary electron beam two of the detectors, which we label ‘left’ and ‘right’, respectively. The reason for this comes from the fact that the sample surface partly blocks electrons from reaching the third detector. The ‘left’ and ‘right’ detectors are arranged symmetrically with respect to the primary beam and the angular acceptance is ± 0.96 rad in the drawing plane and ± 0.4 rad perpendicular to it. For a non-normal incidence, we employ three detectors, which increases the angular acceptance to ± 1.57 rad in the drawing plane, while maintaining a value of ± 0.4 rad perpendicular to it. We will label the detectors ‘left’, ‘center’ and ‘right’ in the following. Delay line anodes allow the determination of the impact position of the electrons. Further, the detectors allow also to recover the impact positions of coincident pairs even if they hit the same detector. These events we may term as ‘double hits’, whereas we refer to ‘single hits’, if the electrons are registered on different detectors. We determine the electron energies via the TOF, where the time reference comes from the pulsed electron gun. The whole set-up is realized in an ultra-high vacuum chamber equipped with standard surface science tools. We define a coordinate system, which has the origin at the sample surface. The y -axis is always parallel to the surface normal, where the x - and z -axes are in-plane. We have chosen the z -axis to be perpendicular to the drawing plane of the geometries. Each coincident event is then characterized by six coordinates, namely the individual energies and pairs of angles Θ and Φ . The total time resolution is approximately 1.8 ns. This will lead to an energy-dependent energy resolution, which is 0.7 eV for a 10 eV electron. We studied a LiF(100) surface, which was kept at a temperature of $\sim 150^\circ\text{C}$ during the measurements to maintain sufficient conductivity. Further, this temperature ensures a clean surface for the duration of the experiment and the annealing of localized electronic defects. The low coincidence count rate required a total acquisition time of ~ 500 h. An electron from the top of the valence band of LiF needs an energy of ~ 13 eV to reach the vacuum level. Therefore, the choice of a primary energy of 30.7 eV ensures that due to energy conservation only one valence band electron and the scattered primary electron can leave the sample. The low kinetic energy cut-off is 2 eV.

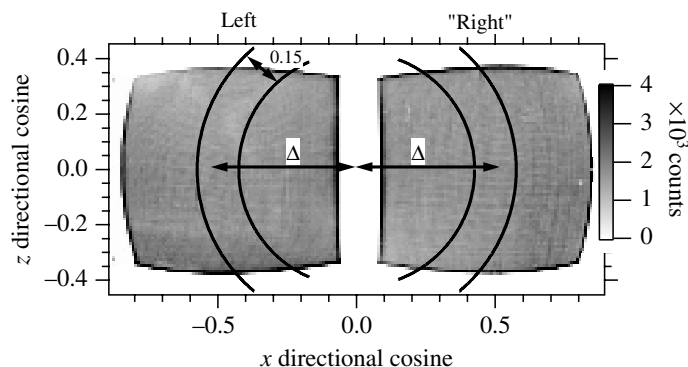


Figure 2. The hit pattern of electron pairs is displayed, where the axes are the directional cosines within the surface. The primary electron hits the surface parallel to the surface normal with an energy of 30.7 eV. The pair of lines on the ‘left’ and ‘right’ detector mark the boundary of narrow regimes. The center has a distance of Δ to the surface normal.

3. Normal incidence excitation

First, we studied the two-dimensional (2D)-energy distributions in the symmetric geometry, where the incident electron beam hits the sample along the surface normal, see figure 1 top. Referring to the detector labeling, we named the electron energies E_{left} and E_{right} , respectively. Implicitly means that we have focussed on ‘single’ hits only. In other words, for each ‘left’ electron there is a ‘right’ counterpart. We know for each coincident event in which direction the individual electrons have left the surface. This emission direction can be characterized by two coordinates and we choose the directional cosines within the surface, which we label as x and z , respectively. In figure 2, we display the hit pattern of the individual electrons of coincident pairs as a function of the directional cosine x and z irrespective of the electron energies. The incident electron beam has an energy of 30.7 eV. In this presentation the coincidence intensity is almost uniformly distributed. It is now interesting to impose a geometrical constraint. More specifically we allow only those emission directions of the ‘left’ and ‘right’ electron such that the included angle between the electron trajectories is essentially fixed and ask for the impact on the energy sharing. A major advantage of the current set-up is that the energy distribution curves can be determined in a post-experiment analysis rather than placing a mask in front of the detectors and performing experiments sequentially. As sketched in figure 2, we define the limited emission directions as follows. On each detector, we define narrow regions by a pair of arcs. They are symmetrically arranged and the mean radius is given by the value of Δ , see figure 2. The difference in radius between the smaller and the larger arc is fixed to 0.15. We allow for a finite width in order to accept enough coincidence events for reasonable statistics. We will consider only those coincidence events where the individual electrons fall within these narrow regimes. We have selected two examples, namely the smallest included angle, this means $\Delta = 0.2$. The largest included angle is obtained for $\Delta = 0.7$. We have plotted the resulting 2D-energy distributions in figure 3. The bars on the right define the color codes for the intensity given in counts. Further we added equidistant contours to the plots². In the case of $\Delta = 0.2$,

² In order to smooth the contour lines we employed a Gaussian filter.

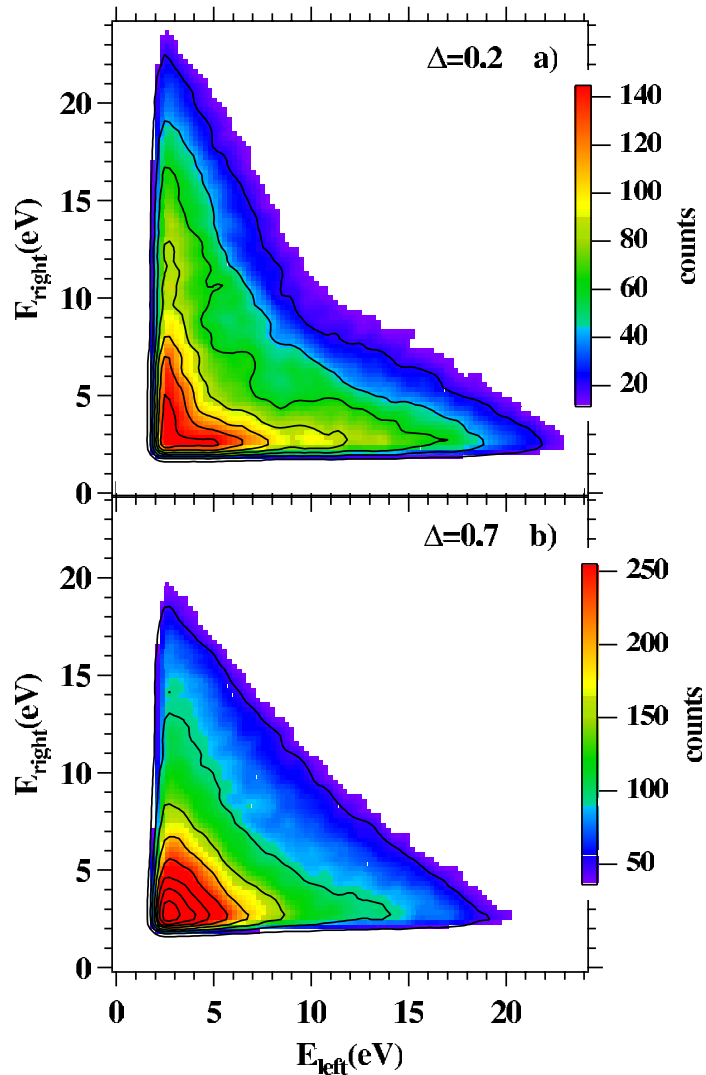


Figure 3. We show the 2D-energy distribution obtained from a LiF(100) surface excited with 30.7 eV primary electrons. In panel (a), we plot the distribution for $\Delta = 0.2$, whereas in panel (b) the result for $\Delta = 0.7$ is displayed.

we note immediately a very unequal energy sharing. Most of the coincidence intensity can be found in two narrow bands parallel to the E_{left} and E_{right} axis resembling the shape of a boomerang. Clearly one electron is essentially confined to energies below ~ 6 eV, whereas the other electron energy can be as high as ~ 18 eV. This means if the included angle between the electrons is small ($\Delta = 0.2$) one electron is ‘fast’ while the other is ‘slow’. If we allow the value of Δ to increase this unequal energy sharing gradually disappears. For $\Delta = 0.7$ the 2D-energy distribution is plotted in figure 3(b). Now the coincidence intensity is essentially constant for constant sum energies $E_{\text{sum}} = E_{\text{left}} + E_{\text{right}}$. The coincidence intensity increases if the sum energy E_{sum} decreases. We learn from figure 3 that electrons which are ‘close’ to each other have very unequal energy sharing, whereas electrons separated by large angles display equal sharing. To emphasize this point we show in figure 4 so-called sharing contributions. These are obtained by choosing a value for E_{sum} and plotting the coincidence intensity as a function of $E_{\text{right}} - E_{\text{left}}$. We

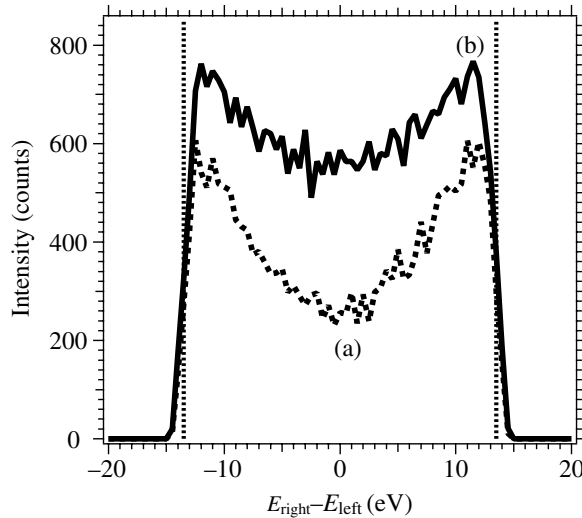


Figure 4. Energy sharing distributions for $E_{\text{sum}} = 17.5 \pm 1$ eV. The curve obtained for $\Delta = 0.2$ is labeled with (a), whereas (b) refers to $\Delta = 0.7$. The vertical dashed lines indicate the positions of the maxima and minima of the energy sharing. These are defined by the low kinetic energy cut-off.

selected $E_{\text{sum}} = 17.5 \pm 1$ eV, which is the highest possible value of E_{sum} for pair emission with a primary beam of 30.7 eV. The curve labeled (a) in figure 4 is obtained from the data shown in figure 3(a), which implies $\Delta = 0.2$. Likewise curve (b) refers to $\Delta = 0.7$. The maximum of curve (a) displays two pronounced maxima at $E_{\text{right}} - E_{\text{left}} \approx \pm 12$ eV. The minimum of curve (a) is at $E_{\text{right}} - E_{\text{left}} \approx 0$ eV and has about half of the intensity of the maxima. It is important to emphasize that the maxima of the sharing function are a result of our low kinetic energy cut-off. We stated above that this value is 2 eV, with this in mind and the chosen maximum sum energy of 17.5 eV, the cut-off occurs at $E_{\text{right}} - E_{\text{left}} = \pm 13.5$ eV. These energy values have been indicated by the vertical dashed lines in figure 4. With a smaller cut-off the sharing distribution would increase further and only if the kinetic energy of one of the electrons approaches zero would the intensity drop. Curve (b) on the other hand shows that the intensity is more uniform though a minimum at $E_{\text{right}} - E_{\text{left}} \approx 0$ eV can be still observed.

4. Non-normal incidence excitation

In the case of ‘double’ hits a meaningful label is to term one electron ‘fast’ and the other ‘slow’ with the energies E_{fast} and E_{slow} , respectively. This implies that $E_{\text{fast}} > E_{\text{slow}}$, consequently we have to label ‘single’ hits in the same fashion. We display the resulting 2D-energy distribution (‘single’ and ‘double’ hits) in figure 5. The bar on the panel defines the color code for the intensity, which is given in counts. Further we added equidistant contours to the plot³. It is apparent that the coincidence intensity is highest in a wedge-shaped region with $E_{\text{slow}} < 4$ eV and $E_{\text{fast}} < 10$ eV. This can be rephrased by saying that there is a preference for one electron being ‘fast’ while the other is ‘slow’. Individual 2D-energy plots including only either ‘single’ or ‘double’ hits reveal that this is due to the contribution of ‘double’ hits. Since those hits occur

³ In order to smooth the contour lines we employed a Gaussian filter.

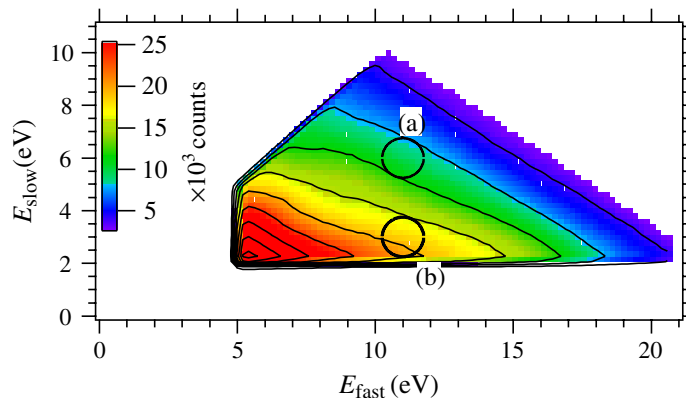


Figure 5. 2D-energy distribution obtained from a LiF(100) surface excited with 30.7 eV primary electrons. One electron of the pair is ‘fast’, whereas the other is ‘slow’ with energies $E_{\text{fast}} > E_{\text{slow}}$. The two circles with radius 0.75 eV indicate energy regions centered at $E_{\text{fast}} = 11$ eV ($E_{\text{slow}} = 6$ eV) and $E_{\text{fast}} = 11$ eV ($E_{\text{slow}} = 3$ eV). Coincident events within these windows are used for 2D-angular plots.

on the same detector we know that the trajectories of these electrons must include smaller angles compared to ‘single’ hits. This aspect will become important later on.

We continue with a 2D-angular presentation of our data. This representation requires the execution of several steps. First, we select values for E_{fast} and E_{slow} , respectively. In order to select enough coincidence events we allow an uncertainty in the energy of ± 0.75 eV. This has been indicated by the circles drawn in figure 5. After the energy selection, we can derive the angular distributions of the ‘fast’ and ‘slow’ electrons. These are not independent of each other, since electron pairs are detected. We would like to emphasize that every ‘fast’ electron has a ‘slow’ counterpart. As an example we show in figure 6 the angular distributions for ‘fast’ and ‘slow’ electrons centered at $E_{\text{fast}} = 11$ eV and $E_{\text{slow}} = 6$ eV (region (a) of figure 2). The intensity is given in counts and the color code is on the right-hand side of the plot. Both distributions display the highest intensity if the electrons leave the sample along the surface normal. The intensity drops for increasing values of $|\Theta|$. We add that the single electron distribution is essentially identical⁴. In the next step, we impose a geometrical constraint. We select only those ‘fast’ electrons, which leave the sample within a narrow angular direction. As an example, we have drawn a black circle in figure 6(b), which is centered at $\Theta = \Phi = 0$ rad. The emission direction is a cone with an angle of 0.18 rad, which is the radius of the circle in figure 6(b). In other words, we fix the direction of the ‘fast’ electron and ask for the intensity of the ‘slow’ electron around this direction. We obtain the intensity map of the ‘slow’ electron displayed in figure 6(c) after normalization to the intensity of the ‘slow’ electron in figure 6(a). This procedure is necessary in order to take into account varying detection efficiencies. It is very clear that the intensity on the center detector is lower than on the left and right detectors. To emphasize this point and to improve the statistics we integrated the data along the Φ direction and show the resulting 1D angular distribution along the Θ direction in figure 6(d). The vertical dashed lines mark the boundary of the allowed Θ values of the ‘fast’ electron. As already evident

⁴ We can determine the single electron distribution by integrating overall E_{slow} values for a given value of E_{fast} .

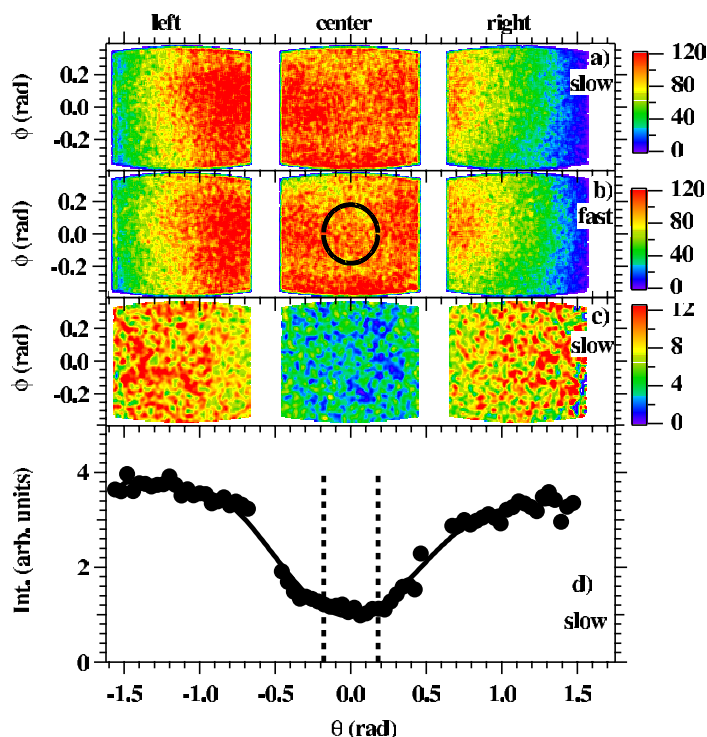


Figure 6. Angular distributions with $E_{\text{fast}} = 11 \text{ eV}$ and $E_{\text{slow}} = 6 \text{ eV}$ are displayed. Panel (a) shows the 2D-angular intensity for the ‘slow’ electron, whereas in panel (b) the same for the ‘fast’ electron is plotted. In panel (c), we plot the intensity for the ‘slow’ electron if the ‘fast’ electron is constrained to be within the area defined by the black circle of the center detector 2 in (b). From panel (c) a line scan can be computed, which is plotted in panel (d). The solid line is a guide to the eye, whereas the dashed vertical lines mark the boundary of the fixed direction.

in figure 6(c), we observe that the ‘fast’ electron is surrounded by a reduced ‘slow’ electron intensity. This is the experimental manifestation of the xc-hole [17, 18]. The key observation is that we are able to show the full extension and shape of the xc-hole. The solid line through the data serves as guide for the eye, the y-axis is in arbitrary units as a result of our normalization procedure. This procedure is the same for all 1D angular distributions to be shown, which facilitates direct comparison. We find that the intensity reaches a constant value at a radius $\Theta \sim 1.2 \text{ rad}$, which is well inside the angular range of our experiment. The position of the maxima may serve as a measure of the xc-hole. It is of course possible to fix the emission direction of the ‘slow’ electron and to determine the intensity map of the ‘fast’ electron. The result of such a presentation is qualitatively and quantitatively identical as far as the size of the depletion zone is concerned. The depletion zone could be observed for different values of E_{fast} and E_{slow} , where the size was independent of the selected energies. We would like to add that we performed some additional experiments utilizing a fourth detector, which was positioned below the ‘center’ detector, see figure 1. These experiments confirmed that the reduced intensity around the fixed emission direction of one electron is also present in the direction perpendicular to the drawing plane of figure 1. We will discuss below under which circumstances, we observe

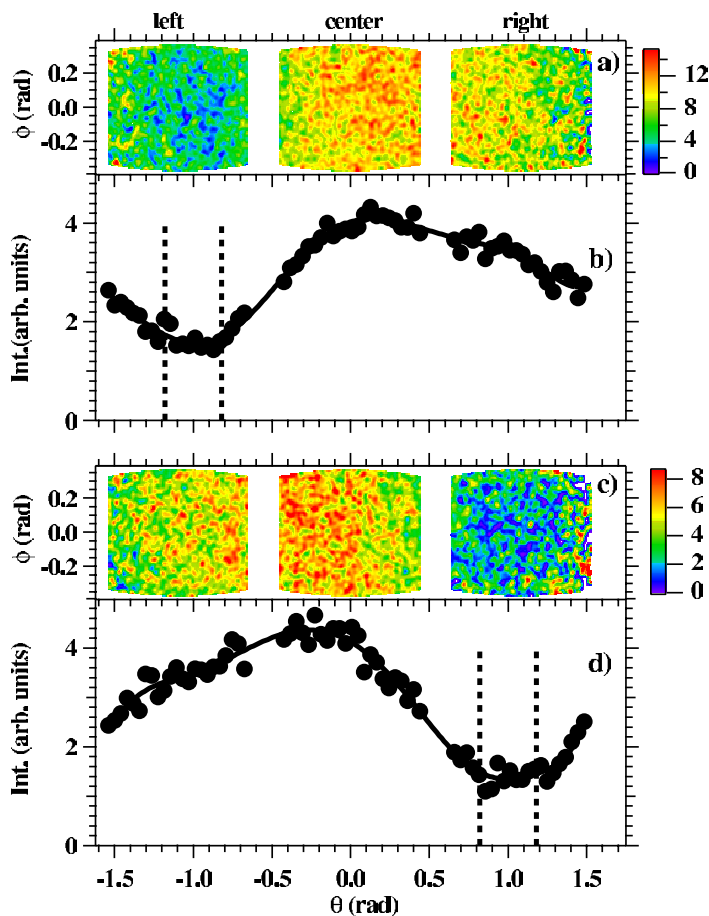


Figure 7. 2D-angular distributions and resulting line scans are shown for electron pairs with $E_{\text{fast}} = 11$ eV and $E_{\text{slow}} = 6$ eV. The direction of the fixed ‘fast’ electron is centered either at $\Theta = -1$ rad for panels (a) and (b) or $\Theta = 1$ rad for panels (c) and (d). The line scans of the intensity maps in (a) and (c) are plotted in panels (b) and (d). The solid lines are a guide to the eye, whereas the dashed vertical lines mark the boundaries of the fixed emission directions.

no xc-hole. The significant advantage of our detection scheme is the ability to select the emission direction of one electron (either ‘slow’ or ‘fast’) anywhere within the angular acceptance. We selected two other emission directions for the ‘fast’ electron. These directions are defined by a circle in the 2D-angular distribution equivalent to figure 6(b), which again has a radius of 0.18 rad. The center is either at $\Theta = -1.0$ rad for figures 4(a) and (b), the case $\Theta = 1.0$ rad is depicted in figures 7(c) and (d). The vertical dashed lines in figures 7(b) and (d) mark the range of the allowed Θ values. We lose the information on the intensity for Θ values on one side of the selected emission direction. However, we gain a larger angular range on the other side. In other words, the maximum angle between the trajectories of the fixed ‘fast’ and ‘slow’ electron is larger in this direction. With the help of the same procedure as employed before we can finally derive the 2D-angular distribution of the ‘slow’ electron around the fixed direction of the ‘fast’ electron. These are plotted in figures 7(a) and (c). In the case of panel (a) we observe a low intensity on the left detector, if we move to the center detector the intensity has increased and

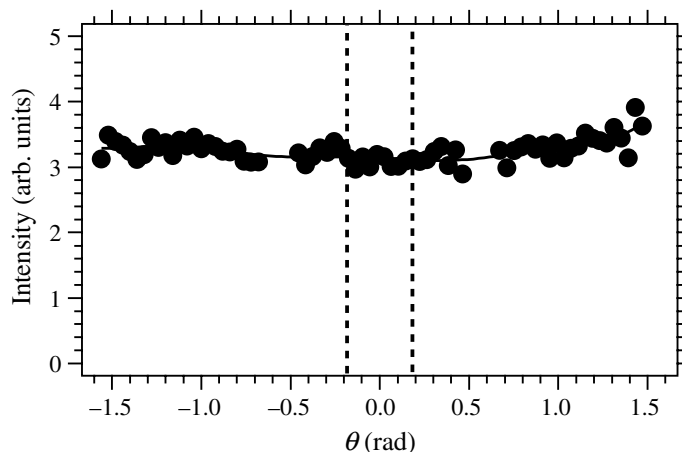


Figure 8. Coincidence intensity for the ‘slow’ electron if the direction of the ‘fast’ electron is fixed at $\Theta = 0$ rad. We selected $E_{\text{fast}} = 11$ eV and $E_{\text{slow}} = 3$ eV. The dashed vertical lines mark the boundary of the fixed direction.

finally the intensity on the right detector is smaller than on the center detector. Again improving the statistics via an integration along the Φ -direction is appropriate and gives a more detailed view, the 1D angular distribution can be seen in figure 7(b). Two important observations can be made. First, we see that the intensity peaks at $\Theta \sim 0.2$ rad, while the ‘fixed’ electron is centered at $\Theta \sim -1.0$ rad. This means that the extension of the depletion zone is ~ 1.2 rad in line with the result shown in figure 6(d). More importantly, we see that the coincidence intensity drops off again if the angle between the two electrons is beyond ~ 1.2 rad. An equivalent situation is observed in figure 7(d) despite the breaking of symmetry. We have to emphasize that the primary beam hits the sample with an angle of 32° , see figure 1. Therefore, we cannot *a priori* expect to observe a symmetric behavior as we do. A closer inspection of the line scans in figures 6 and 7 reveal a hint of symmetry breaking. In figure 6(d) the maximum for negative Θ values is slightly larger than for positive Θ values (3.8 versus 3.4 arbitrary units). Comparing figures 7(b) and (d) shows that the maximum for negative Θ values is larger than the maximum for positive Θ values (4.1 versus 4.5 arbitrary units). We can clearly see that the reduced intensity regime follows the fixed emission direction. As an example of a vanished xc-hole we display in figure 8, the intensity of the ‘slow’ electron as a function of Θ . The fixed emission direction of the ‘fast’ electron is located at the center detector like the case depicted in figure 6(b). The energies are centered at $E_{\text{fast}} = 11$ eV and $E_{\text{slow}} = 3$ eV, respectively. These are the events which are located within region (b) in the 2D-energy plot of figure 5. This choice ensures that we are in the regime where there is a preference of one electron being ‘fast’ while the other is ‘slow’. We have explained this to be due to the 2D-energy distribution of the ‘double’ hits. In this case the trajectories of the electrons include small angles, hence they are ‘close’ to each other. This is consistent with the effect of a geometrical constraint on the 2D-energy distribution as discussed in section 3. It was observed that if the electrons are forced to be close to each other ($\Delta = 0.2$) one electron carried most of the available kinetic energy. If we consider now the emission direction of either ‘fast’ or ‘slow’ fixed, the counterpart shows additional intensity for trajectories close to the fixed emission direction. The net effect is that the xc-hole will be ‘filled’ and an essentially constant intensity as a function of Θ is observed. This filling of the xc-hole

occurs gradually if we vary E_{slow} from 6 to 3 eV. More specifically the size of the xc-hole stays essentially constant, but the minimum is filled up. This observation is directly linked to the 2D-energy distribution of coincidence events. Additionally, we point out that 3 eV electrons are part of the secondary electron tail. These electrons have encountered more than one collision event. The net result is then that the coherence with the ‘fast’ electron is lost. Consequently, we should not expect to observe a depletion zone. From the above made comments it becomes obvious that the vanishing depletion zone is not related to the difference in sum energy of the data shown in figures 6 and 8, respectively. As a matter of fact choosing $E_{\text{fast}} = 14$ eV and $E_{\text{slow}} = 3$ eV, where the sum energy is identical to the data plotted in figure 6, still yields no depletion zone.

5. Discussion

From the experimental data obtained in the symmetric geometry, we learn that the angle between the trajectories has a strong influence on how the available energy is shared among the electrons. We found that if this angle is small the electrons tend to avoid having the same kinetic energy and most of the coincidence intensity is found for one electron having most of the energy of the pair, see figures 3 and 4. On the other hand, for large angles between the trajectories we observe a more equal energy sharing. A simple picture of the electron–electron scattering, where the interaction between the electrons is mediated by a screened Coulomb interaction, shows that if the trajectories are forced to be close to each other one electron is ‘fast’ while the other is ‘slow’. The introduction of a screened Coulomb potential follows (within the concept of the xc-hole) from the missing electronic charge surrounding each electron (due to the Pauli principle and Coulomb interaction). This is a valid approach following the experimental evidence employing the non-normal incidence geometry. The angular distribution of the coincidence intensity around the fixed emission direction of one electron clearly shows a depletion zone, see figures 6 and 7. Our angular acceptance of the instrument is large enough to fully map this region. This fact constitutes the major advance of our work. Due to the size of the depletion zone, which is about 1.2 rad, it is also justified to allow the fixed direction to be rather large (0.18 rad). We have found no significant variation of the angular size of the depletion zone for other values of E_{fast} and E_{slow} . This is also true for data sets obtained with different excitation energies. Of course this means that in momentum space the depletion zone size will scale with the square root of the energy. The size of the depletion zone is a measure of the electron–electron interaction inside the solid. It would be desirable to compare our experimental depletion zone size with theory. This is, however, beyond the capability of current solid state theory. Experimentally, we plan to systematically study the depletion zone for different materials. For example, how does the present result of an insulator compare with a typical metal, e.g. Cu? In general two electrons tend to avoid each other leading to the concept of the xc-hole. Our experiments confirm this picture as long as the individual energies E_{fast} and E_{slow} are not too unequal as just shown.

6. Summary

The concept of the xc-hole was introduced more than 70 years ago and is an essential part of modern solid state theory. Our results clearly demonstrate that it is an experimental reality beyond being an important theoretical concept and shows up as a depletion zone in the angular distribution of the coincidence intensity. Specifically, we have proven that we can fully map

the depletion zone in angular space. We find for the size obtained from electrons originating from a LiF(100) surface a value of ≈ 1.2 rad independent of the energy of the electrons. We also discovered a correlation in energy space proven by the disappearance of the xc-hole if the electron energies are very unequal. It would be now a challenge for theory to use our angular distributions results and solve the so-called inverse problem of scattering. In other words, to derive the scattering potential, which essentially is the key function $\mathbf{n}_{xc}(\mathbf{r}, \mathbf{r}')$. This may serve as a basis for an improvement of the DFT beyond the LDA.

Acknowledgments

We acknowledge the expert assistance in the construction and operation of the experiment by H Engelhard and D Hartung.

References

- [1] Drude P 1900 *Ann. Phys. Lpz.* **306** 566–613
- [2] Lorentz H A 1909 *The Theory of Electrons* (Leipzig: BG Teubner)
- [3] Sommerfeld A 1927 *Naturwissenschaften* **15** 63
- [4] Wigner E and Seitz F 1933 *Phys. Rev.* **43** 804
- [5] Slater J C 1934 *Rev. Mod. Phys.* **6** 209
- [6] Hohenberg P and Kohn W 1964 *Phys. Rev.* **136** B864
- [7] Kohn W and Sham L J 1965 *Phys. Rev.* **140** A1133
- [8] Kohn W 1998 *Rev. Mod. Phys.* **71** 1253
- [9] Fulde P 1993 *Electron Correlations in Molecules and Solids* (*Springer Series in Solid State Sciences* vol 100) (Berlin: Springer)
- [10] Alonso J A and Girifalco L A 1978 *Phys. Rev. B* **17** 3735
- [11] Krüger P, Wolfgarten G and Pollmann J 1985 *Solid State Commun.* **53** 885–9
- [12] Puzder A, Chou M Y and Hood R Q 2001 *Phys. Rev. A* **64** 022501
- [13] Rushton P P, Tozer D J and Clark S J 2002 *Phys. Rev. B* **65** 235203
- [14] Constantin L A, Perdew J P and Tao J 2006 *Phys. Rev. B* **73** 205104
- [15] Nekovee M, Foulkes W M C and Needs R J 2003 *Phys. Rev. B* **68** 235108
- [16] Rutherford E 1911 *Phil. Mag.* **21** 669
- [17] Schumann F O, Kirschner J and Berakdar J 2005 *Phys. Rev. Lett.* **95** 117601
- [18] Schumann F O, Winkler C, Kerhervé G and Kirschner J 2006 *Phys. Rev. B* **73** 041404(R)
- [19] McCarthy I E and Weigold E 1991 *Rep. Prog. Phys.* **54** 789
- [20] Vos M and McCarthy I E 1995 *Rev. Mod. Phys.* **67** 713
- [21] Iacobucci S, Marassi L, Camilloni R, Nannarone S and Stefani G 1995 *Phys. Rev. B* **51** R10252
- [22] Inokuti M 1971 *Rev. Mod. Phys.* **43** 297
- [23] Kirschner J, Artamonov O M and Samarin S N 1995 *Phys. Rev. Lett.* **75** 2424
- [24] Feder R, Gollisch H, Meinert D, Scheunemann T, Artamonov O M, Samarin S N and Kirschner J 1998 *Phys. Rev. B* **58** 16418
- [25] Samarin S, Berakdar J, Artamonov O M and Kirschner J 2000 *Phys. Rev. Lett.* **85** 1746
- [26] Berakdar J, Gollisch H and Feder R 1999 *Solid State Commun.* **112** 587
- [27] Gollisch H and Feder R 2004 *J. Phys.: Condens. Matter* **16** 2207
- [28] Rucker U, Gollisch H and Feder R 2005 *Phys. Rev. B* **72** 214424
- [29] Gollisch H, Schwartzberg N V and Feder R 2006 *Phys. Rev. B* **74** 075407